



High-performance C/C composites derived from phthalonitrile matrix CFRP via a few cycles of vacuum-assisted impregnation-carbonization

Vladislav Aleshkevich^{*}, Oleg Morozov, Alexander Babkin, Alexey Kepman, Boris Bulgakov

M.V. Lomonosov Moscow State University, Department of Chemistry, Division of Chemical Technology and New Materials, Leninskie Gory St, 1-11, 119991 Moscow, Russia

ARTICLE INFO

Keywords:

C/C composites
Phthalonitrile
Carbonization
Graphitization

ABSTRACT

Novel approach of fabrication of carbon-carbon composites from carbon fiber reinforced plastics with phthalonitrile matrices was presented. Polymer composites were obtained by vacuum infusion, carbonized, and reimpregnated with following carbonization to reduce porosity of the resulting materials. The highest mechanical properties and lowest porosity were obtained when CFRP post-cured at 375 °C was taken initially. 4 cycles of impregnation-carbonization are sufficient to fabricate materials with the highest properties. Phthalonitrile resin transformations through curing, carbonization and graphitization using XRD, Raman spectroscopy, elemental analysis, FTIR and solid-state NMR were researched. TGA-MS revealed exposure of CH₄, NH₃, H₂O, HCN, benzene and phenol gases during carbonization. Amorphous carbon materials were obtained after carbonization at 1000 °C with I_D/I_G = 2.38 and graphitization at 2200 °C resulted in formation of more structured carbon material with I_D/I_G = 0.63. Mechanical and thermal properties of the composites were determined at every step of the process.

1. Introduction

Carbon-carbon (C/C) composites are a class of materials composed of carbon fibers and a carbon matrix. They are widely known for their strength and durability, as well as for their resistance to extreme temperatures and corrosion [1–3]. These properties have made them ideal for high-performance applications in the aerospace, chemical, and medical industries [4–6].

One of the most advanced modern C/C manufacturing approaches is the carbonization of carbon fiber reinforced polymers (CFRP) [7–9]. In this approach usually thermosetting matrix of the composite converts to carbon through slow heating. During this process, non-carbon atoms are eliminated, resulting in the formation of a porous carbon material. These pores can then be filled by reimpregnating with the resin and further carbonization, and, for specific purposes, they might be filled using chemical vapor deposition of carbon from a gas phase. The most common carbon sources used in C/C manufacturing nowadays are phenolic resins and charcoal pitch [7,10]. Both approaches require high pressure and temperature applications [11,12]. Therefore, a search of new carbon sources for C/C composites fabrication has perspectives for applications and could reveal new insights into the structural transformations

of different thermosetting matrices into carbon.

Phthalonitrile resins are known for being the most heat resistant thermosets for polymer composites fabrication [13,14]. This aspect has provided their application in various fields, such as in ray shielding materials [15–17], structural composites in aerospace [18–20], micro-electronic packaging [15,21,22], ballistics [23,24] and other high-tech applications [25–29]. Curing of the phthalonitrile resins is usually initiated by aromatic amines or phenols, resulting in the formation of the aromatic structures, such as isoindoline, phthalocyanine and triazine [30–34]. Highly cross-linked polymeric networks built with these aromatic structures provide the thermosets with high thermal stability (T_{5%} > 500 °C) and the retention of their mechanical properties at elevated temperatures [35–38] and after thermal-oxidative aging [39,40]. Along with high heat resistance, thermosets exhibit char yield values over 70 % [14,41], as well as low shrinkage upon pyrolysis [42]. These factors combined lead to the formation of a uniform and dense carbon matrix [27,43]. The single studies aimed to apply phthalonitriles as precursors for carbon matrices have been reported since the late 1990-s [42,44,45]. However, in this aspect, phthalonitrile resins have not been comprehensively studied, due to complications with CFRP fabrication [46,47]. CFRPs were made using solution impregnation process, because of the

^{*} Corresponding author.

E-mail address: vladislav.aleshkevich@gmail.com (V. Aleshkevich).

<https://doi.org/10.1016/j.compositesa.2024.108201>

Received 10 January 2024; Received in revised form 21 March 2024; Accepted 7 April 2024

Available online 9 April 2024

1359-835X/© 2024 Elsevier Ltd. All rights reserved.

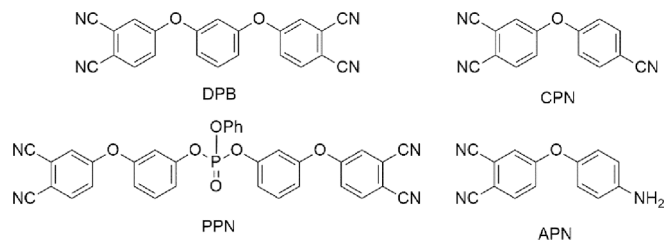


Fig. 1. Monomers of the PN resin.

resin high melting temperature and viscosity. However, this process does not allow further reimpregnation. The density of these obtained carbonized CFRPs varies from 1.36 to about 2.00 g/cm³. Due to these issues, recent works have studied theoretical aspects of phthalonitriles pyrolysis [29,48–51], as well as the functional applications of phthalonitrile-derived carbon materials, such as semiconductors, CO₂ adsorbents and supercapacitor electrodes [29,52,53].

After revealing phthalonitrile formulations, that allow the fabrication of the composites using cost-effective injection methods, such as vacuum infusion molding process (VIMP) and resin transfer molding (RTM) [54–57], phthalonitriles have recently gained attention as a promising carbon source for the manufacturing of structural carbon–carbon composites [27,43]. These works studied composites derived from easy-processable phosphate-containing phthalonitrile formulations in carbonization [57,58], and the resulting C/C composites demonstrated prospective physical properties for applications. Unlike phenolic resins and charcoal pitch, the use of phthalonitriles does not require the application of high pressure, yielding in lower processing time and costs [27,43]. This approach allowed the fabrication of C/Cs without the need for high-pressure equipment and with a total process time below a few weeks. Even after 2 cycles of carbonization-reimpregnation, the materials exhibited performance comparable to C/Cs, fabricated with phenolic resins. A growing demand for the application of phthalonitrile resins in the production of carbon materials has attracted our interest in an in-depth fundamental study of the transformations occurring in phosphorus-containing resins during carbonization. The reported studies of phthalonitriles pyrolysis were aimed at revealing evolving gasses and kinetics [50,51,59] and did not deepen concern about changes occurring in the matrix. The phosphate-containing comonomer PPN provides the necessary processability to the resin, however, it can also impact the formation of the carbon matrix during carbonization and graphitization. Thus, the present study reveals transformations that took place in the phthalonitrile matrix during the carbonization process along by solid state CP-MAS NMR, elemental analysis, Raman spectroscopy and XRD with characterization of the resulting carbon materials to provide new insights into the synthesis of carbon matrices from polymeric materials by cost-efficient technologies.

2. Experimental details

2.1. Materials

Phthalonitrile resin PN, suitable for the impregnation process, was purchased from Itecm (Russia). The resin contains monomer bis(3-(3,4-dicyanophenoxy)phenyl) phenylphosphate (PPN, Fig. 1), as a viscosity-reducing agent, according to the manufacturer. The thermosets properties, crucial for the present study, are given in Fig. S1.

2.2. Characterization

Melt viscosity was measured with a Physica MCR 302 according to GOST 57950-2017.

Differential scanning calorimetry (DSC) was performed on a DSC TA Q20 at a heating rate of 10 °C/min under a nitrogen atmosphere.

Thermal stability was evaluated using thermogravimetric analysis (TGA) on a thermal analyzer STA 449 F5 Jupiter coupled with a quadrupole mass spectrometer QMS 403C Aeolos at a heating rate of 10 °C/min over the range 40–1000 °C and Ar purge rate of mL/min.

The glass transition temperature (T_g) was measured using the 3-point bending method on a DMA Q800 dynamic mechanical analyzer according to GOST 56753–2015.

Carbon and hydrogen mass content were measured using an express-gravimetric method. Nitrogen content was measured using the Dumas method. A 3–5 mg sample was combusted on granulated NiO in oxygen flow at 1000 °C in the presence of PbO. The evolved CO₂ and H₂O gases were absorbed with ascarite and anhydron respectively. The carbon and hydrogen masses were calculated from the absorbers weight gain. Nitrogen detection was carried out using a thermal conductivity detector.

Phosphorus mass content was measured on a Cary-100 spectrophotometer. 2–5 mg sample was combusted in oxygen atmosphere at 1000 °C. The formed phosphorus oxide was transferred into solution as blue phosphomolybdate complex.

X-ray diffraction (XRD) patterns were recorded on a Bruker D8 Advance X-Ray diffractometer with a Cu K α anode ($\lambda = 1.5418 \text{ \AA}$) operating at 40 kV and 40 mA. The diffraction patterns were collected at 25 °C and over an angular range of 10 to 50° with a step size of 0.05° per step.

Raman spectra were recorded on a HORIBA Raman Spectrometer with a wavelength 514 nm.

Fourier Transform Infrared (FTIR) spectra were recorded on a Bruker Tensor 27 FTIR with a DLATGS detector in the range of 3200–400 cm⁻¹ using KBr pellets.

The solid-state ¹³C and ³¹P MAS NMR spectra were recorded on a BRUKER AVANCE-II NMR 400 WB spectrometer with a magnetic field of 9.4 T using a 4 mm H/X/Y MAS WVT probe (spinning rate is 10 kHz). The direct polarization (DP) pulse sequences were combined with high-power proton decoupling. The swept frequency two-pulse phase modulation (SW-TPPM) sequence ($\tau = 8 \mu\text{s}$, $\phi = 15^\circ$) was used for proton decoupling.

Tensile strength ($^+\sigma$) and tensile modulus (^+E) were measured with a Tinius Olsen 300ST according to GOST 56785–2015. Compressive strength ($^-\sigma$) and compressive modulus (^-E) were measured with a Tinius Olsen 300ST according to GOST 56812–2015. Interlaminar shear strength (ILSS, $\tau_{1,3}$) was measured with a Tinius Olsen 50ST according to GOST 32659–2014. Flexural strength (σ_f) and flexural modulus (E_f) were measured with a Tinius Olsen H5K-S according to GOST 56810–2015.

Micrographs were taken on a Tescan Vega 3 at an accelerating voltage of 20 kV.

“Hydrostatic” density (ρ_w) was measured using hydrostatic weighing method with an analytical balance Vibra ht-220-CE according to GOST 15139–69. Volumetric density (ρ_v) was measured on samples with dimensions 20 × 10 × 2 mm³ by dividing mass of the dried at 150 °C for 1 h sample by its exact dimensions. Open porosity was calculated using the following equation:

$$\text{Porosity} = \left(1 - \frac{\rho_v}{\rho_w}\right) \times 100\%$$

Mercury porosimetry measurements were made using a Micromeritics AutoPore V 9605. The sample was first evacuated to a pressure of 20 mm Hg at 150 °C to remove sorbed water from the interior of the sample. Mercury intrusion was held at room temperature.

Specific heat capacity was measured with a DSC 214 Polyma according to GOST 56754. Thermal diffusivity was measured with a LFA 457 MicroFlash according to ASTM E1461 normally. Thermal conductivity (λ) was calculated using the following equation:

$$\text{Thermal conductivity} = \text{Thermal diffusivity} \times \text{Heat capacity} \times \text{Density}$$

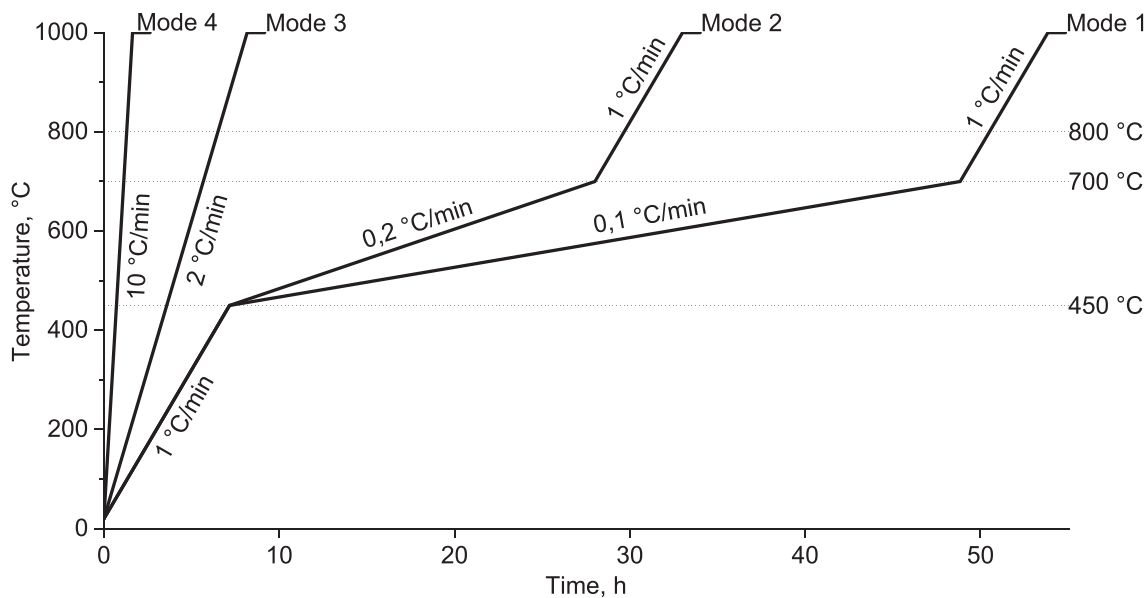


Fig. 2. Carbonization modes. (For interpretation of the references to colour in this figure legend, the reader is referred to the web version of this article.)

Table 1
Sample names.

Name	Preparation procedure
PN-180	PN resin, cured at 180 °C
PN-375	PN resin, post-cured at 375 °C
PN-1000	PN-375, carbonized at 1000 °C with carbonization mode 1
PN-2200	PN-1000, graphitized at 2200 °C for 3 h
CFRP-330	Carbon fiber reinforced PN resin, post-cured at 330 °C
CFRP-350	Carbon fiber reinforced PN resin, post-cured at 350 °C
CFRP-375	Carbon fiber reinforced PN resin, post-cured at 375 °C
CFRP-400	Carbon fiber reinforced PN resin, post-cured at 400 °C
C/C-330	CFRP-330, carbonized at 1000 °C with carbonization mode 1
C/C-350	CFRP-350, carbonized at 1000 °C with carbonization mode 1
C/C-375	CFRP-375, carbonized at 1000 °C with carbonization mode 1
C/C-400	CFRP-400, carbonized at 1000 °C with carbonization mode 1

2.3. Polymer samples preparation

Solid resin PN was placed in a 3 L glass reactor. The resin was heated to 130 °C and vacuumed to a constant pressure while stirring. The degassed liquid resin was poured into a metal mold (450 × 270 × 2 mm). Curing was carried out by heating at 2 °C/min up to 180 °C and dwelling for 8 h (PN-180). After that, the cured resin plate was post-cured according to the following program: rapid heating to 180 °C (2 °C/min), slow heating (10 °C/h) from 180 °C to 375 °C with a dwelling for 8 h at this temperature (PN-375).

2.4. Carbon fiber reinforced plastic (CFRP) samples preparation

CFRPs were prepared by vacuum infusion and cured in a vacuum bag. A solid resin PN was placed in a 3-liter glass reactor. The resin was heated to 130 °C and vacuumed at constant pressure while stirring. The obtained liquid resin was poured into a metal container, from which it was subsequently fed through a hose into a pre-assembled bag with carbon fiber. The reinforcement for the manufacture of CFRPs was a 22,502 carbon fabric manufactured by JSC INUMiT with a density of 200 g/m², twill 2 × 2, UMT42S-3K-EP 3K carbon fiber. Ten 30 × 30 cm² fabric sheets laid out in one direction were used for each composite. The container and vacuum bag were kept in a heat chamber at 130 °C (infusion temperature). After complete impregnation of the fiber (30–40 min), the heat chamber with vacuum bag was heated according

to the following mode: heating 2 °C/min to 180 °C, followed by dwelling for 8 h at 180 °C.

After initial curing the composite was post-cured freestanding in a metal box filled with fine powder coke according to the following program: heating to 180 °C (2 °C/min), dwelling for 30 min at 180 °C, heating 5 °C/h to stated temperature (from 330 to 400 °C) with dwelling for 8 h at this temperature, cooling 10 °C/h to 100 °C.

2.5. Carbonization

CFRP specimens were placed into a metal box filled with fine char powder. The box was placed into a furnace with a connected system for purging the chamber with dry nitrogen. The nitrogen flow rate was adjusted to create an overpressure in the furnace, as determined by the bubble device at the furnace outlet. Heating was performed according to the modes shown in Fig. 2.

2.6. C/Cs reimpregnation

Reimpregnation of porous C/C specimens was performed using the same methods as described in Section 2.4, except that the C/C specimen was used instead of the carbon fabric preform.

2.7. Graphitization

Graphitization was performed in a vacuum furnace with the following heating mode: heating at 10 °C/min to 2200 °C, followed by dwelling at 2200 °C for 3 h.

All the sample names are listed in Table 1.

3. Results and discussion

3.1. Polymer composites fabrication

A phthalonitrile resin PN was chosen as an available easy-processable PN resin suitable for vacuum infusion (Fig. S1). The resin consisted of a common phthalonitrile monomer DPB, curing agent APN and reactive diluents CPN and PPN providing the desired processability to the formulation. In preliminary experiments, specimens of thermosets were obtained and post-cured at various temperatures: 330 °C, 350 °C, 375 °C and 400 °C. It is known that an increase in the curing

Table 2
Properties of the post-cured PN thermosets.

Test characteristic	PN-330	PN-350	PN-375	PN-400
σ_f , MPa	143.5 ± 6.8	105.7 ± 7.6	63.5 ± 6.7	51.8 ± 8.7
E_f , GPa	4.1 ± 0.1	4.3 ± 0.1	4.0 ± 0.1	4.4 ± 0.1
T_g , °C	356	379	>450	>450
ρ_{Wf} , g/cm ³	1.32 ± 0.01	1.34 ± 0.01	1.35 ± 0.01	1.35 ± 0.01
Y_c , Ar, 1000 °C, %	69.2	70.7	72.6	74.3

temperature leads to a simultaneous increase in $T_{5\%}$ and char yield of the thermosets, along with a decrease in mechanical properties and transversal cracking in composites [14]. The same trends were observed for the studied resin, indicating an increase in the cross-linking density of the thermosets with an increase in the curing temperature (Table 2). The TGA experiments revealed char yields in a range of 69–74 % (Table 2, Fig. 3A) for all thermosets, making them promising matrices for C/C composites fabrication. Given that mechanical performance and initial cross-linking density may influence the resulting material, it was decided to analyze four different post-curing temperatures for CFRP in C/C fabrication.

CFRP specimens were prepared by vacuum infusion process. The impregnation step was performed at 130 °C, followed by curing at 180 °C in a vacuum bag and free-standing post-curing at 4 different temperatures (330, 350, 375 and 400 °C). The resultant CFRPs contained 37.0 ± 2.0 wt% of resin and were tested for their mechanical properties. Similar to the thermosets, it was found that the composite's mechanical performance decreases as the post-cure temperature increases (Table 3). This is attributed to an increased degree of resin crosslinking, which caused the CFRP to shrink and internal stresses to appear. This leads to the formation of microcracks at higher post-cure temperatures (CFRP-375 and CFRP-400) (Fig. 4). These microcracks are perpendicular to the carbon fiber layers and are uniformly distributed throughout the volume of the specimens. CFRP shrinkage is determined by two factors: matrix chemical transformations and thermal effects within the material [60]. An increase in chemical crosslinks with increasing post-curing temperature leads to an increase in matrix

density (Table 2). On the other hand, different coefficients of thermal expansion of the matrix and carbon fibers generate even higher internal stresses within the CFRP after the heating and cooling processes. When the critical point of internal stress has been reached, the structure relaxes and a free surface is formed. For carbonization, this factor might play a positive role in the mechanical properties and integrity of the C/C composite because channels formed by microcracks can serve for elimination of pyrolysis gases without further destruction of the matrix.

3.2. CFRP carbonization

The CFRP carbonization process was carried out in a nitrogen atmosphere using the following heating mode, described earlier [27]: heat 20 → 450 °C, 1 °C/min; 450 → 700 °C, 0.1 °C/min; 700 → 1000 °C, 1 °C/min; dwell at 1000 °C, 1 h. This mode is based on the TGA results which indicated that most active mass loss occurs between 450–700 °C (Fig. 3). From DTG curves it can be seen that the highest degradation rate occurs at between 450 °C and 700 °C.

The obtained samples were studied by mechanical tests and mercury porosimetry. Table 4 shows that after carbonization, the ILSS values of the composites drastically decreased in comparison to CFRP. At the same time, C/C materials derived from CFRP post-cured at higher temperatures (C/C-375 and C/C-400) demonstrated higher mechanical strength values, than C/C, derived from CFRP post-cured at lower temperatures

Table 3
Properties of the post-cured CFRPs.

Test characteristic	CFRP-330	CFRP-350	CFRP-375	CFRP-400
$^+\sigma$, MPa	885,1 ± 28,5	729,9 ± 39,9	664,9 ± 24,2	651,8 ± 30,9
^+E , GPa	73,2 ± 2,0	71,1 ± 1,8	70,2 ± 0,6	71,6 ± 2,1
$^-\sigma$, MPa	672,5 ± 35,8	575,3 ± 30,7	535,1 ± 53,7	528,9 ± 22,2
^-E , GPa	73,5 ± 3,4	64,2 ± 5,3	64,4 ± 6,0	60,4 ± 1,3
τ_{13} , MPa	51,9 ± 2,1	42,2 ± 2,3	34,2 ± 1,2	21,9 ± 1,7

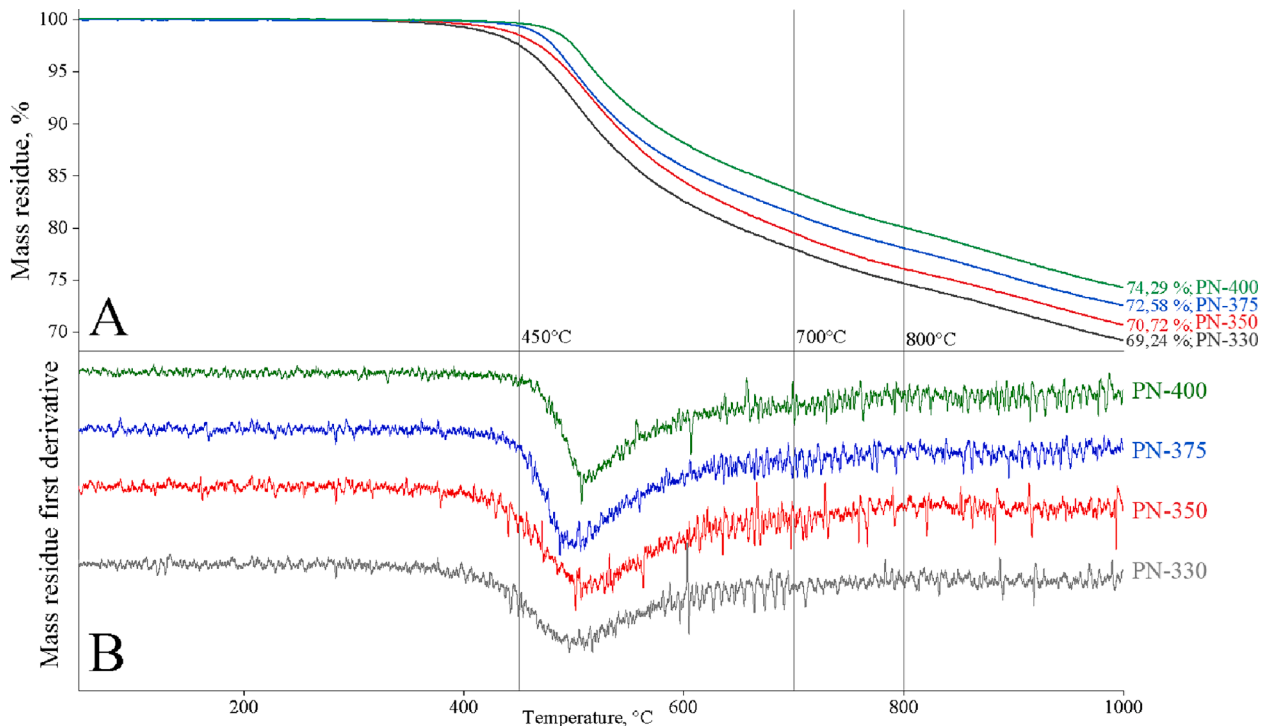


Fig. 3. TGA curves (A) and its first derivatives (B) for PN-330 (gray), PN-350 (red), PN-375 (blue) and PN-400 (green). (For interpretation of the references to colour in this figure legend, the reader is referred to the web version of this article.)

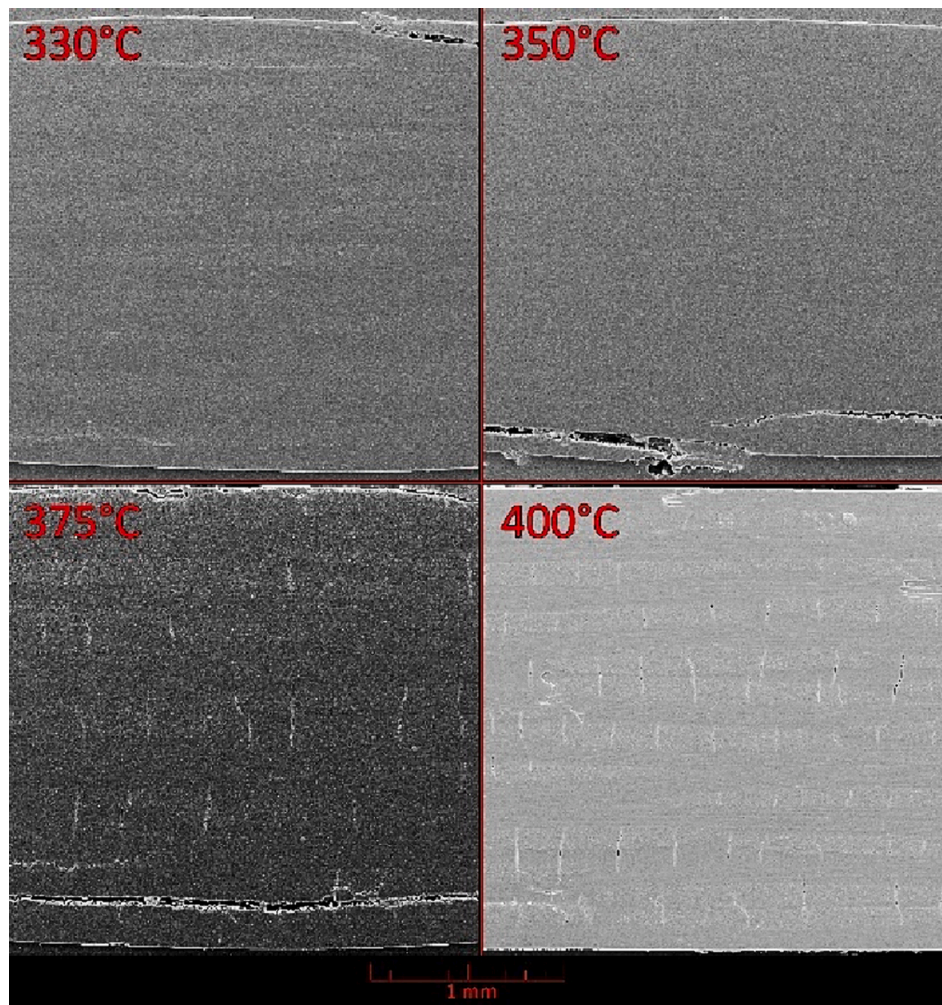


Fig. 4. SEM images of the CFRPs post-cured at different temperatures. (For interpretation of the references to colour in this figure legend, the reader is referred to the web version of this article.)

Table 4
Characteristics of C/C derived from CFRP, post-cured at different temperatures.

	Cycle	C/C-330	C/C-350	C/C-375	C/C-400
τ_{13} , MPa	1	5.58 ± 0.66	5.90 ± 0.51	6.60 ± 0.40	6.74 ± 0.36
	2	6.65 ± 0.74	6.55 ± 0.42	8.30 ± 0.63	8.19 ± 0.57
Porosity, %	1	20.34 ± 1.28	16.43 ± 0.32	16.42 ± 0.64	17.38 ± 0.70
	2	6.5 ± 0.81	6.2 ± 0.45	6.2 ± 0.9	6.5 ± 0.51
ρ_V , g/cm ³	1	1.37 ± 0.02	1.37 ± 0.01	1.37 ± 0.01	1.36 ± 0.02
	2	1.51 ± 0.02	1.51 ± 0.02	1.52 ± 0.02	1.50 ± 0.02
ρ_W , g/cm ³	1	1.72 ± 0.01	1.64 ± 0.01	1.64 ± 0.01	1.65 ± 0.01
	2	1.62 ± 0.02	1.61 ± 0.02	1.62 ± 0.02	1.61 ± 0.01

(C/C-330 and C/C-350). Except for the C/C-330, the porosity and density values are approximately the same for all C/Cs after the first cycle, which can be explained by the lowest heat resistance (T5%) of this thermoset among the studied ones. All C/C samples were reimpregnated with the same phthalonitrile resin using a similar procedure. Pores were filled with the liquid resin, which can be clearly seen in the SEM images (Fig. 5). After the second cycle of carbonization, C/C-375 and C/C-400 showed higher ILSS, compared to C/C-330 and C/C-350. Supposedly, the microcracks in the initial composites served as outlets for pyrolytic gases in C/C-375 and C/C-400. On the contrary, in C/C-330 and C/C-350, the gas evolution process in the material occurred with a chaotic destruction of the matrix structure. In the latter case, the voids formed are larger and less uniformly distributed (Fig. S4), which significantly

affected the mechanical performance of the materials (Table 4).

Composites were investigated for porosity to evaluate the morphology of the materials. The differently sized pores volume comparison showed a clear dependence between the pore diameter and its ability to be filled with phthalonitrile resin (Fig. 6). The volume of pores with diameters greater than 6 μm decreased dramatically after the 2nd cycle (Table S1). In addition, the presence of more uniformly distributed pore tunnels in C/C-375 and C/C-400 provided a better impregnation ratio. There are no significant variations in the properties of C/C-375 and C/C-400, and for this reason, the application of post-curing at 400 °C had been considered excessive, and further research was conducted on CFRP-375.

3.3. Carbonization mode optimization

In a further set of experiments CFRP-375 was carbonized using four different heating modes, including mode 1, which had been used in the previous set of experiments (Fig. 2). Since earlier reports had concluded that longer heating does not affect the properties of the composites, the faster TGA modes 2–4 were taken into consideration. Modes 1–2 were based on TGA data, indicating that majority of mass loss occurs at 450–700 °C (Fig. 3). The carbonized samples were then tested for their mechanical performance and morphology.

Large voids were clearly visible in the SEM image of the C/C composite obtained using Mode 1 (Fig. 7). This indicates that most of the mass loss in this sample is due to the matrix cracking and spalling,

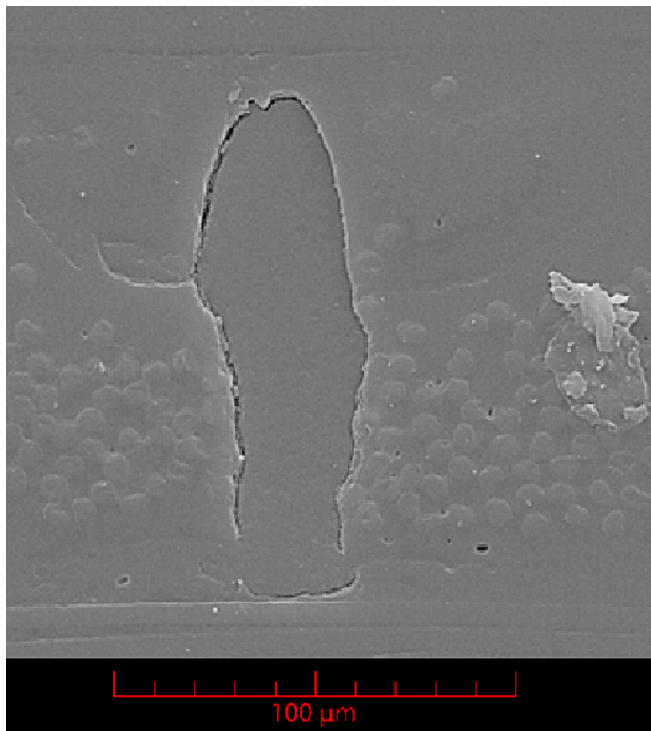


Fig. 5. SEM image of filled pore. (For interpretation of the references to colour in this figure legend, the reader is referred to the web version of this article.)

caused by rapid gas evolution, rather than the removal of non-carbon atoms or chemical structure rearrangement. There are no noticeable differences between the SEM images of the C/C composites, obtained with Modes 1–3. A comparison of the measurable properties for the C/Cs in Modes 1–3 indicated no significant differences after either the first, or the second cycle (Tables 5, S2; Fig. 8). Only pores with diameters greater than 6 μm are filled during the second impregnation-carbonization cycle. The increased intrusion volume of C/C in Mode 4 is explained by a large number of cracks. Therefore, reducing the heating rate in the temperature interval of the greatest mass loss does not result in a material with a different morphology or better performance. However, rapid heating may result in material destruction. Therefore, all subsequent carbonizations were performed using Mode 3 with a constant heating rate of 2 K/min.

3.4. Study of multiple reimpregnation-carbonization cycles and graphitization

To develop a new method for the fabrication of low-porous C/C composites from phthalonitrile-based CFRP, five cycles of impregnation-carbonization were performed. The increase in mass gain after each impregnation step was monitored to estimate the saturation of the composite with the resin. As can be seen in Fig. 9, the mass gain per cycle significantly decreased from the 2nd to the 4th cycle. No mass gain was observed in the 5th cycle, indicating that no additional porosity had been filled, and the 5th cycle was excessive.

Mercury porosimetry was used to evaluate the morphology of the composites. After each cycle, the pore volume decreased dramatically (Fig. 10, Table S3) and the mechanical strength of the material increased (Tables 6, S4). Additionally, pore filling resulted in a more uniform

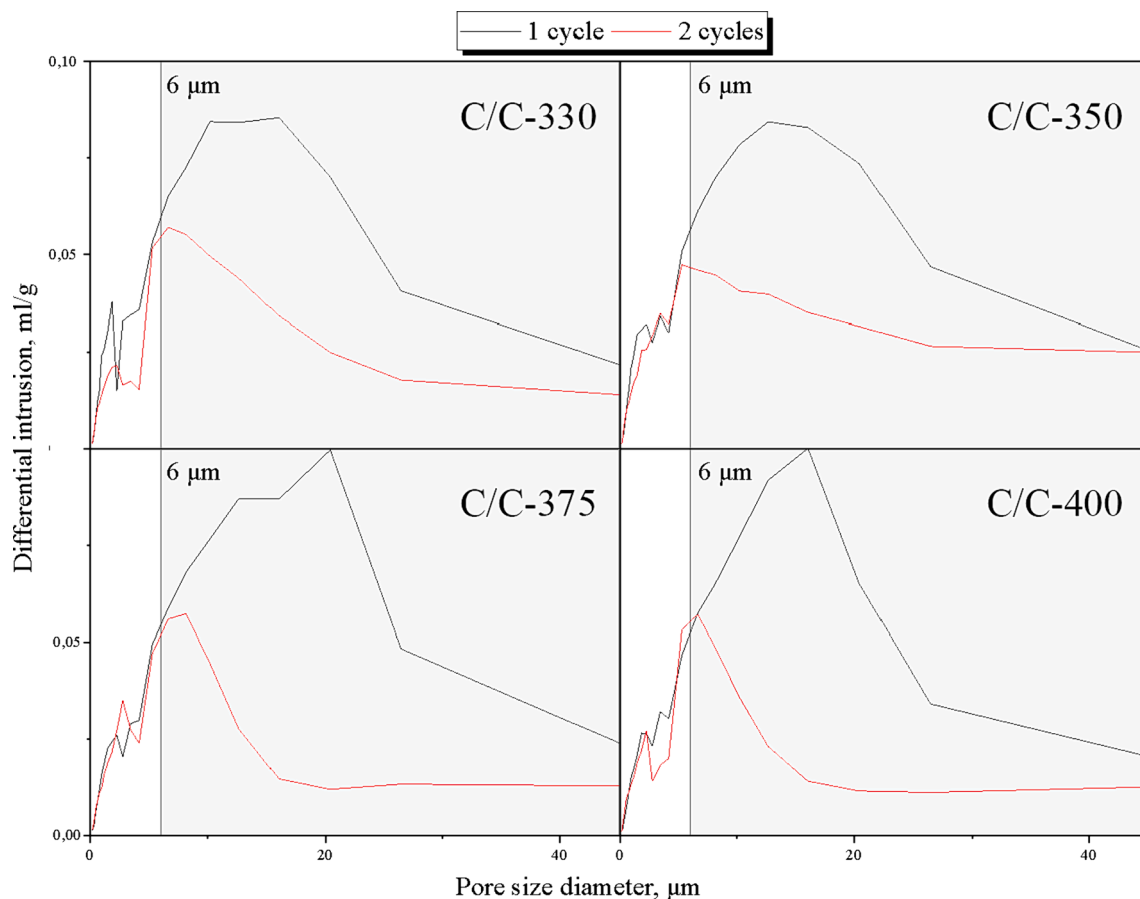


Fig. 6. Mercury porosimetry data of C/C derived from CFRP, post-cured at different temperatures. (For interpretation of the references to colour in this figure legend, the reader is referred to the web version of this article.)

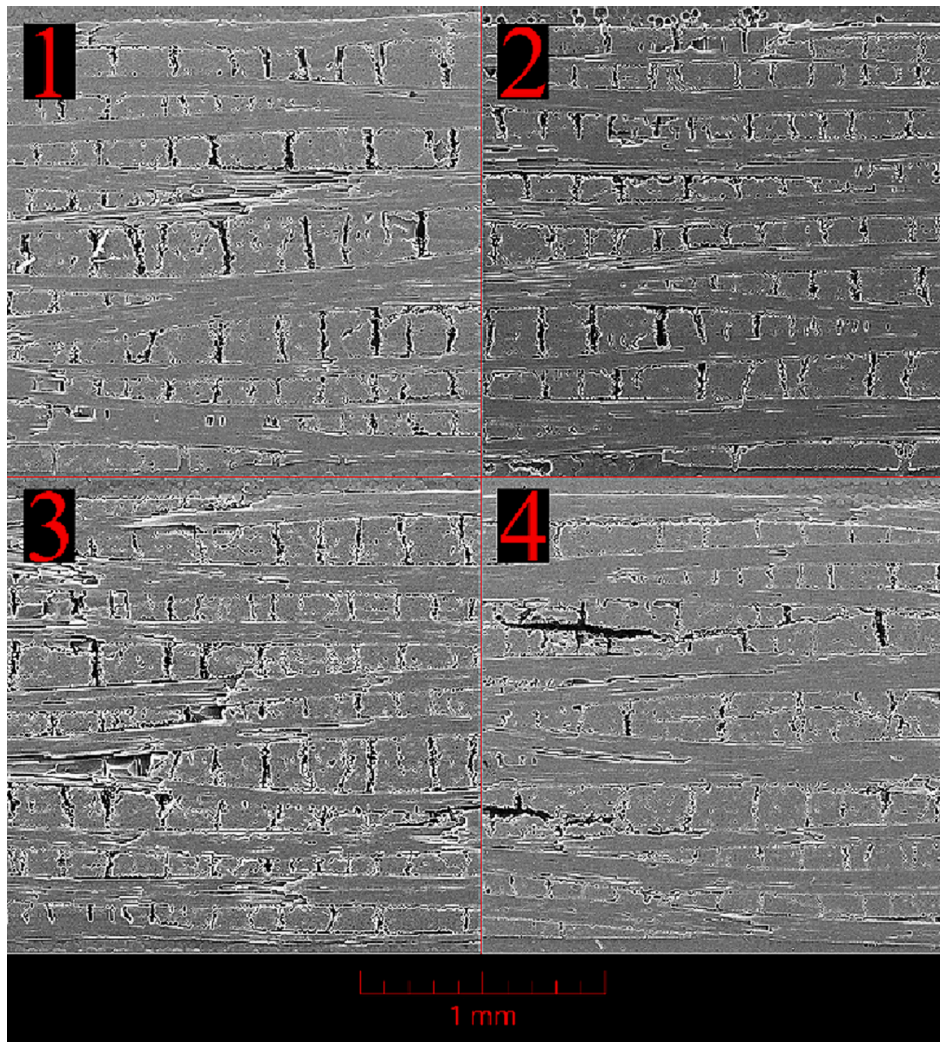


Fig. 7. SEM images of C/Cs, manufactured with different heating modes, after 1st cycle. (For interpretation of the references to colour in this figure legend, the reader is referred to the web version of this article.)

Table 5
Characteristics of C/C derived with different carbonization modes.

		Mode 1	Mode 2	Mode 3	Mode 4
τ_{13} , MPa	1	6.6 ± 0.4	6.5 ± 0.1	6.6 ± 0.4	5.6 ± 0.3
	2	8.7 ± 0.6	7.7 ± 0.5	8.6 ± 0.6	7.4 ± 0.3
Porosity, %	1	16.4 ± 0.6	15.9 ± 0.9	15.8 ± 0.6	16.7 ± 0.7
	2	6.2 ± 0.9	7.4 ± 1.7	6.2 ± 1.1	7.9 ± 1.4
ρ_V , g/cm ³	1	1.37 ± 0.01	1.38 ± 0.01	1.38 ± 0.01	1.37 ± 0.01
	2	1.52 ± 0.01	1.51 ± 0.01	1.52 ± 0.01	1.49 ± 0.02
ρ_W , g/cm ³	1	1.64 ± 0.01	1.64 ± 0.01	1.64 ± 0.01	1.65 ± 0.01
	2	1.62 ± 0.01	1.63 ± 0.01	1.62 ± 0.01	1.62 ± 0.01

material with higher thermal properties, which is crucial for heat transfer in aircraft brakes [61].

Further heat treatment at 2200 °C was carried out to remove non-carbon atoms from the structure. The resulting structure showed even better thermal performance due to the more graphite-like carbon matrix formation (Tables 7, S5). Further non-carbon atoms removal leads to higher porosity values and, as a result, a decrease in some mechanical strength values. However, it should be noticed, that C/Cs flexural strength nearly doubled after graphitization. It can be explained by the increased synergy between the graphitized fiber and the matrix.

It should be noted that a direct comparison of different C/C composites can only offer a possible range of properties for C/C composites

due to the use of different reinforcements in each case. The mechanical properties of the composites before graphitization surpass the values for composites obtained from other precursors after just the third cycle. It is worth noting the simplicity of the fabrication process and the significantly lower porosities of the materials obtained in the present work. The use of phenolic resin or pitch as a carbon source in C/Cs production requires either the use of hot-pressing prepregs (10–30 bar at 200–250 °C) with subsequent carbonization of the resulting CFRP, or high isostatic pressure carbonization directly from carbon fiber and pitch (up to 1000 bar at 600–800 °C). It can be seen that the use of phthalonitrile resins in the production of C/Cs not only results in similar properties of the materials, but also allows to use a more cost-efficient approach: vacuum infusion method. This allows to significantly reduce the price and processing time without requiring the use of high pressure as needed when phenolics or pitch are used. Moreover, the obtained C/Cs have lower porosity, which is crucial for brakes or thermal shielding.

3.5. Chemical transformations in the phthalonitrile matrices during C/C composites synthesis

The carbon structure of the resulting material highly depends on the carbon source; this structure was synthesized from [65]. To trace the transformations occurring in the thermoset during heat treatment, a series of structural analyses was carried out. For this purpose,

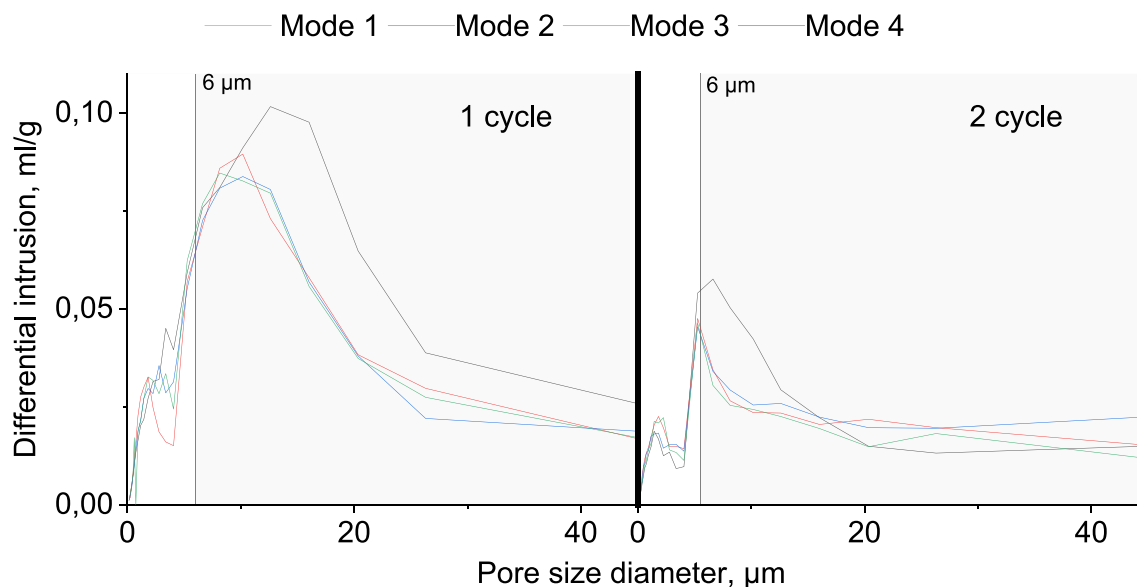


Fig. 8. Mercury porosimetry data of C/C derived with different carbonization modes. (For interpretation of the references to colour in this figure legend, the reader is referred to the web version of this article.)

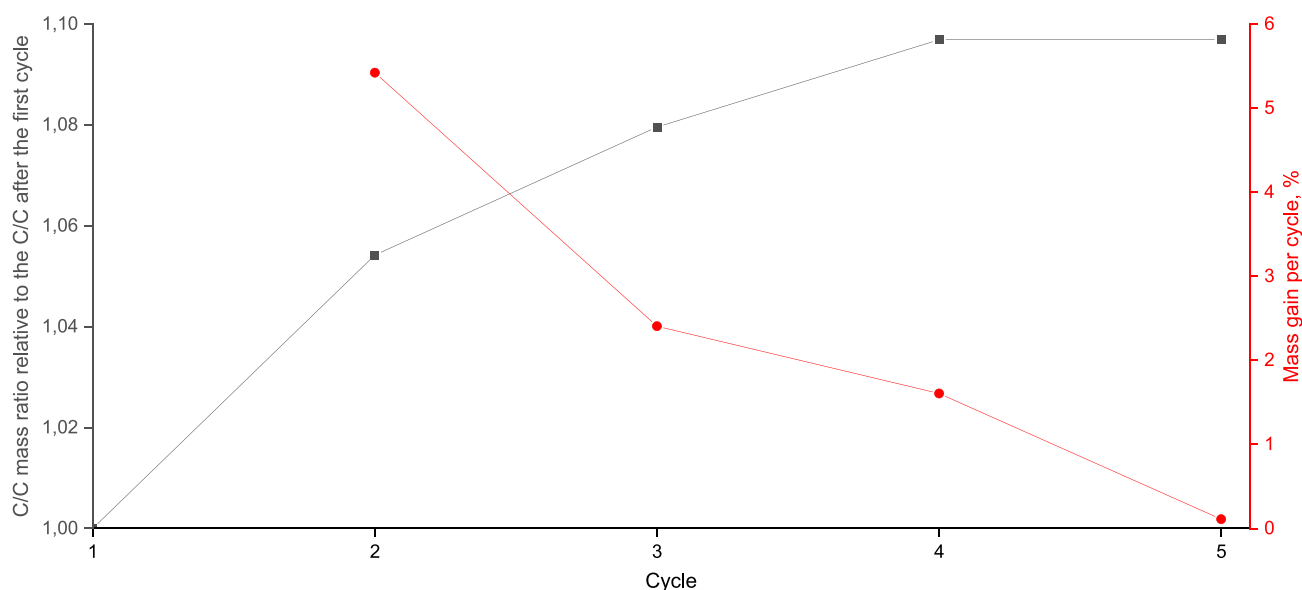


Fig. 9. Mass change (black) and mass gain of C/C per cycle (red) of repeated impregnation-carbonization. (For interpretation of the references to colour in this figure legend, the reader is referred to the web version of this article.)

thermosets were prepared from the resin, cured, and post-cured. Changes that occur in the polymer structure during curing and post-curing are observed in infrared spectra (Fig. 11). A small peak at 1010 cm^{-1} can be seen in the spectra of both cured (PN-180) and post-cured (PN-375) thermosets, corresponding to the presence of phthalocyanine fragments [66], the peak at 1360 cm^{-1} indicates the presence of triazine rings and peaks at 1525 and 1708 cm^{-1} — isoindoline units [67]. Since only one cyano group of phthalonitrile is involved in the triazine cycle formation, the peak at 2223 cm^{-1} (cyano group) remains present in all post-cured polymer (Figure S9). The carbonization of the thermosets led to a significant increase in carbon content in the resulting structure, due to the evolving pyrolytic gases, which are mainly composed of non-carbon atoms. In the spectrum of PN-1000, the peaks presented in non-carbonized samples are absent, indicating that there are no nitrogen-containing heterocycles or residual cyano-groups remaining. Two significant peaks in this spectrum are located at 1093

cm^{-1} ($\text{P} = \text{O}$) and 1635 cm^{-1} ($\text{C} = \text{C}$). The former indicates the remaining initial state of the phosphorus fragment and the latter is attributed to the formation of a graphene-like structure. There are no significant peaks in the IR spectrum of PN-2200. Weak signals in $800\text{--}1600\text{ cm}^{-1}$ can be related to stretching of carbon-carbon bonds.

In addition to FTIR studies, the chemical structure of resin PN after post-curing at $375\text{ }^\circ\text{C}$ was further characterized using solid-state ^{13}C and ^{31}P NMR (Fig. 12). In the ^{13}C spectrum two wide peaks were observed. The peak at 117.27 ppm is attributed to nitrile carbon [68], which correlates with IR data. A group of overlapping peaks at 135.01 ppm is attributed to aromatic carbon atoms, and at 158.58 ppm , attributed to triazine structure carbon atoms [68]. The latter signal disappeared after a carbonization treatment at $1000\text{ }^\circ\text{C}$, indicating the destruction of nitrogen-containing heterocycles and a rearrangement in polyaromatic carbon structure. The only peaks in the ^{13}C spectrum of the PN-1000 and PN-2200 were broadened due to the high anisotropy of forming

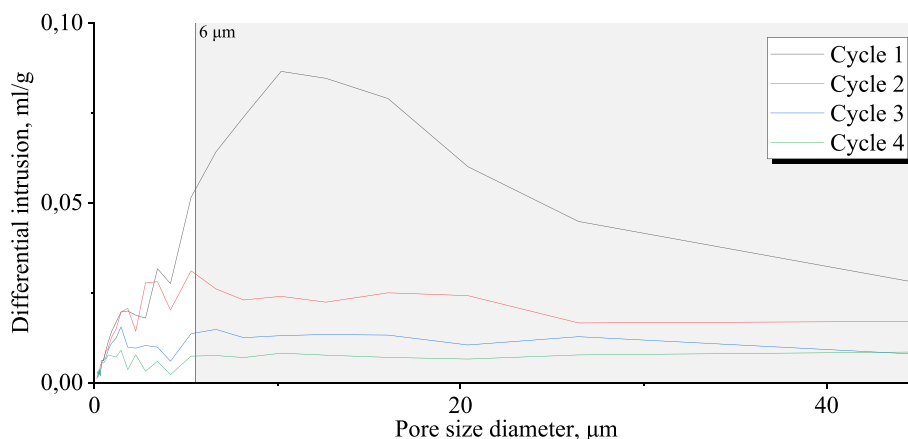


Fig. 10. Mercury porosimetry data of C/C after different cycles count. (For interpretation of the references to colour in this figure legend, the reader is referred to the web version of this article.)

Table 6
Mechanical characteristics of C/Cs.

	Cycle				Literature data		
	1	2	3	4	Phthalonitrile [27,43]	Phenolic resin [62,63]	Pitch [63,64]
τ_{13} at 25 °C, MPa	6.6 ± 0.4	8.7 ± 0.6	12.1 ± 1.3	15.6 ± 1.3	4.6–7.9	6.2–18.0	12.6–20.0
$^+\sigma$ at 25 °C, Mpa	61.0 ± 16.1	47.3 ± 8.3	45.5 ± 8.1	63.7 ± 14.8	–	–	–
$^-\sigma$ at 25 °C, Mpa	96.3 ± 10.3	104.2 ± 6.6	182.8 ± 16.4	279.3 ± 34.3	72.2–139.8	35.3–148.0	72.2–200
σ_f at 25 °C, Mpa	57.4 ± 8.0	69.9 ± 7.6	98.0 ± 9.5	143.7 ± 9.1	–	110	100–180
Porosity, %	15.8 ± 0.6	6.2 ± 1.4	4.9 ± 0.5	4.3 ± 0.4	21.94–22.19	14.0–16.0	7.0–12.1
ρ_V , g/cm ³	1.38 ± 0.01	1.52 ± 0.01	1.54 ± 0.01	1.55 ± 0.01	–	1.2–1.3	1.2–1.5
ρ_W , g/cm ³	1.64 ± 0.01	1.62 ± 0.01	1.62 ± 0.01	1.62 ± 0.01	1.53–1.72	1.58–1.77	1.67–1.7
λ , W/m-K	1.01 ± 0.02	1.33 ± 0.03	1.73 ± 0.05	2.34 ± 0.06	–	–	–

Table 7
Mechanical characteristics of C/C after different cycles count with final graphitization.

	Cycle			
	1	2	3	4
τ_{13} at 25 °C, MPa	5.5 ± 0.6	6.9 ± 0.8	8.7 ± 1.0	12.5 ± 1.4
$^+\sigma$ at 25 °C, MPa	169.3 ± 20.2	152.9 ± 18.2	157.4 ± 11.2	135.9 ± 6.2
$^-\sigma$ at 25 °C, MPa	73.6 ± 3.5	104.1 ± 6.9	147.3 ± 1.6	163.8 ± 6.7
σ_f at 25 °C, MPa	121.6 ± 13.0	163.0 ± 5.9	231.6 ± 10.5	272.4 ± 18.1
Porosity, %	21.0 ± 0.9	12.5 ± 0.7	8.2 ± 0.6	6.3 ± 0.8
ρ_V , g/cm ³	1.39 ± 0.02	1.51 ± 0.01	1.55 ± 0.02	1.57 ± 0.02
ρ_W , g/cm ³	1.76 ± 0.01	1.73 ± 0.01	1.70 ± 0.02	1.68 ± 0.01
λ , W/m-K	1.16 ± 0.04	5.24 ± 0.18	6.47 ± 0.29	8.62 ± 0.31

graphene-like structure. The only strong line associated with the aromatic carbon [1–3] was found.

The ³¹P NMR spectrum of uncured resin has only one signal corresponding to the PPN monomer (Figure S3) [57]. Two signals at –4.63 and –12.71 ppm are present in all three solid state spectra, indicating that the phosphorus structure remains in the form of λ^5 -phosphanes (mainly in the form of orthophosphate) [69,70]. Considering that phosphates can transform into polyphosphates at high temperatures [71], condensed phosphates should be considered the most likely form of phosphate-like structure [40,72,73]. No signals are present in the ³¹P spectrum of PN-2200, indicating no phosphorus remains in the structure after graphitization process.

The chemical composition was also characterized by elemental analysis (Table 8). The obtained data showed that all nitrogen atoms were eliminated from the polymer matrix during the carbonization

process, which correlates with ¹³C NMR data, indicating the destruction of nitrogen-containing heterocycles. The contents of hydrogen and other atoms, mostly formed by oxygen, decreased with a significant increase in the content of carbon and phosphorus. During further graphitization, all non-carbon atoms were eliminated from the sample, resulting in a pure carbon structure after graphitization. It should be noted that phosphorus atoms remain in the PN-1000 structure presumably in forms of polyphosphates [73] and are removed only after the graphitization process at PN-2200 [40].

The carbon structure formed after carbonization at 1000 °C and graphitization at 2200 °C were studied using X-ray diffraction analysis (Fig. 13) and Raman spectroscopy (Fig. 14). A peak found for PN-2200 was narrower and shifted closer to the graphite (002) reflection. The interlayer spacing d_{002} and the crystallite size along the c-axis (L_c) were calculated from XRD, and the relative intensities I_D/I_G of the Raman bands and crystallite size along the a-axis (L_a) are shown in Table 9. The structure of PN-2200 was more ordered compared to that of PN-1000. Moreover, the Raman bands of PN-2200 were more resolved, and the intensity ratio of D/G bands was lower than that of PN-1000. This indicates that the structural defects in carbon had been healed during the graphitization process, forming a more ordered structure. It should be noted, that due to the high aromaticity of the polymer network the resulting structure of carbonized phthalonitrile is more ordered, compared to carbonized phenolic resins ($I_D/I_G = 3.15$ after 1000 °C treatment) [74] and corresponds with carbonized phthalonitriles from the previous publications [17,53]. Moreover, despite the presence of residual phosphorus atoms in PN-1000, the resulting structure is fairly ordered, with a further improvement after the graphitization and a complete elimination of phosphorus. Additionally, the use of phthalonitrile monomers with phosphorus fragments in the monomer composition significantly lowers the viscosity of the resin. This allows application of the highly efficient vacuum infusion method not only for

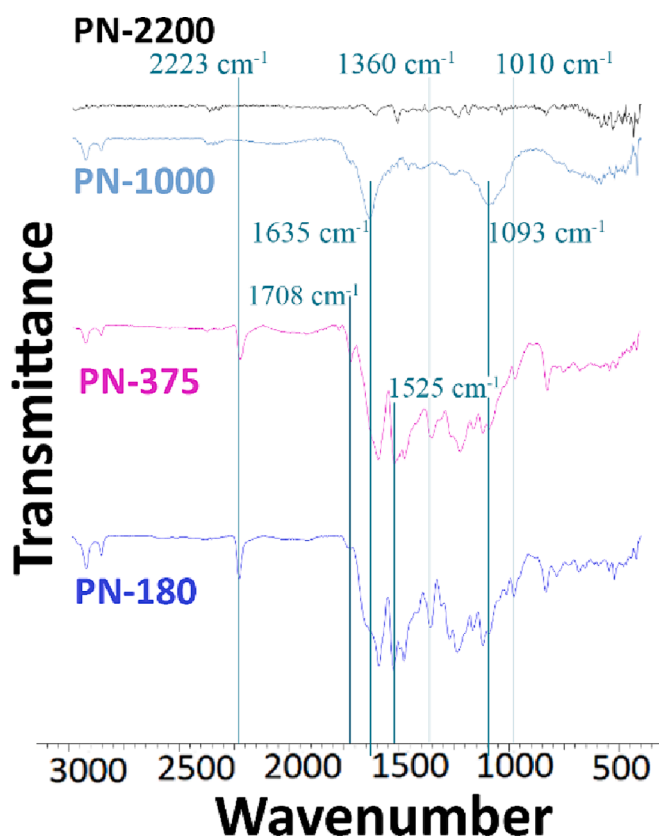


Fig. 11. FTIR transmittance spectra of thermosets, processed at different temperatures. (For interpretation of the references to colour in this figure legend, the reader is referred to the web version of this article.)

the CFRP fabrication but also for the reimpregnation of porous C/Cs.

As mentioned above, non-carbon-atoms containing gases evolved from the polymer during the carbonization process. To characterize these gases and the temperature range of the most intense gas evolution, thermogravimetric analysis (TGA) with mass spectrometry of the evolving gases was performed (Figs. 3, 15). The ion currents of the evolved gases showed the presence of CH_4 , NH_3 , H_2O , HCN , CO_2 , benzene, and phenol gases which corresponds with the previous publications [39,50,51,57,59,75]. Methane gas evolution started at 455°C with a signal maximum at 572°C due to the pyrolysis of heteroatomic structures (phthalocyanine and triazine), benzene ring cleavage and polycondensation reaction [76,77]. The evolution of NH_3 takes place between 490 and 700°C and is mainly due to the decomposition of a curing additive [39]. HCN evolution, on the other hand, occurs in a narrower temperature range (489 – 684°C) and can be interpreted as the removal of unreacted cyano groups [50]. The formation of H_2O is associated with hydroxyl groups [76] and occurs between 450 and 700°C . The evolution of CO_2 is mainly due to the cleavage of oxygen-containing functional groups [78]. The formation of phenol and benzene responds to the cleavage of the bridged C–O–C bond with the release of a low molecular weight product [50].

Table 8
Elements contents for resins PN after heat treatment.

Element content, mass. %	PN	PN-180	PN-375	PN-1000	PN-2200
C	72.3 ± 0.3	72.2 ± 0.3	72.9 ± 0.3	92.2 ± 0.4	100
H	3.3 ± 0.1	3.2 ± 0.1	3.5 ± 0.1	0.8 ± 0.1	0
N	15.5 ± 0.1	12.9 ± 0.1	11.4 ± 0.1	0	0
P	0.7 ± 0.1	0.6 ± 0.1	0.9 ± 0.1	6.6 ± 0.3	0
Other atoms	8.2 ± 0.4	11.1 ± 0.4	11.3 ± 0.4	0.4 ± 0.3	0

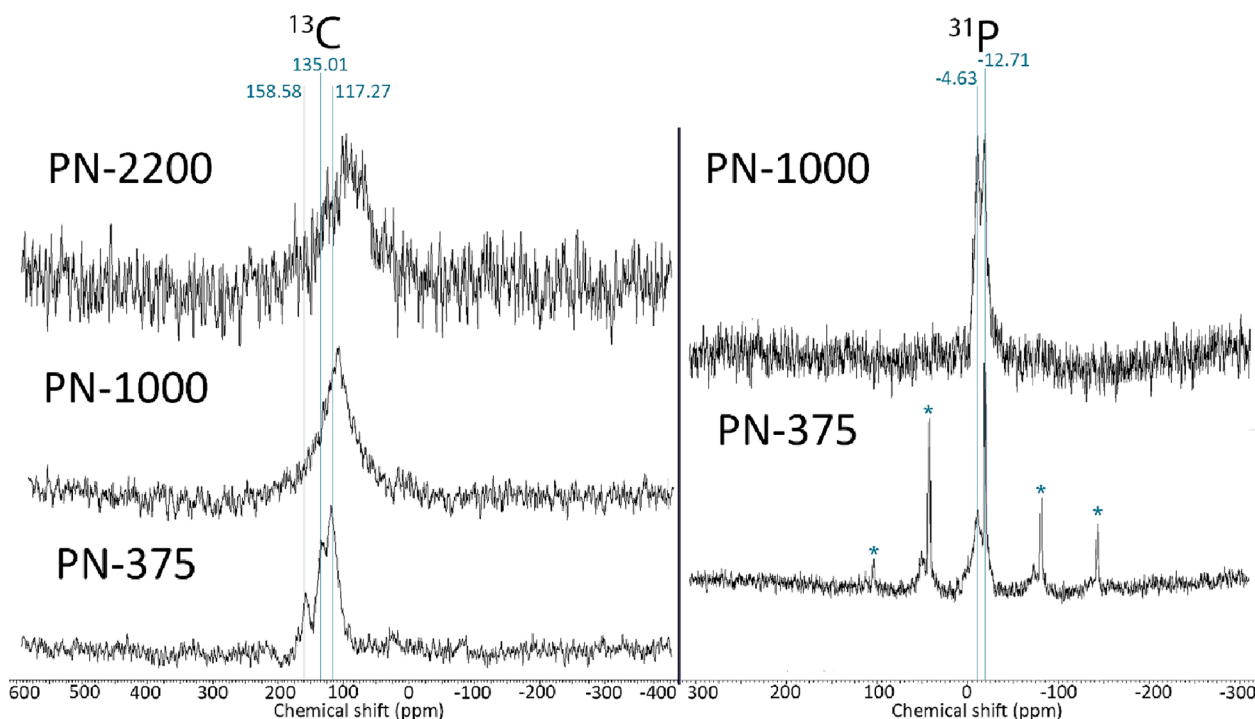


Fig. 12. Solid-state ^{13}C (left) and ^{31}P (right) NMR for thermoset after different heat treatment. Asterisks denote spinning sidebands. (For interpretation of the references to colour in this figure legend, the reader is referred to the web version of this article.)

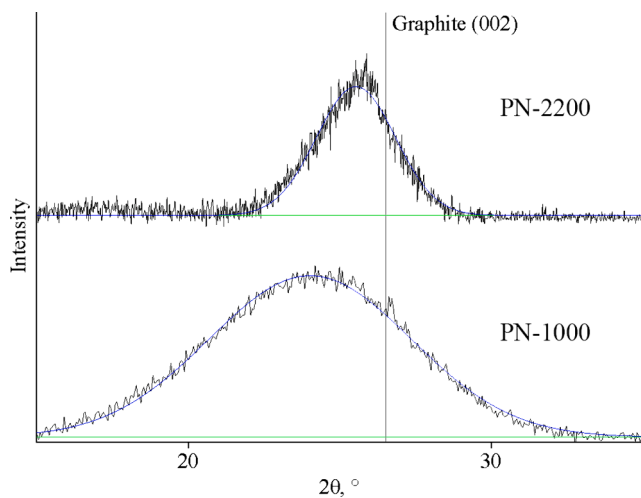


Fig. 13. The X-ray diffraction patterns of PN-1000 and PN-2200. (For interpretation of the references to colour in this figure legend, the reader is referred to the web version of this article.)

4. Conclusions

This paper illustrates the performance of phthalonitrile resin as a carbon source in the preparation of C/C composites. A novel cost-efficient energy-saving approach for the C/C composites fabrication by the multiple steps of preform impregnation in a vacuum bag has been presented. It has been shown that the choice of post-cure temperature for the initial CFRP does not affect the resulting chemical structure of the matrix, but only determines the morphology of the composites. The presence of pore channels in the CFRP preform facilitates gas evolution and results in more uniformly distributed pores in the final C/C composite. Therefore, a post-curing temperature of 375 °C has been established as optimal for the CFRP post-curing prior to carbonization. Pores with diameters greater than 6 μm have been reimpregnated up to 4 times with the same resin in order to obtain a material with improved performance and reduced porosity. Subsequent reimpregnation did not result in porosity filling. Furthermore, using heating modes with extra-low heating rates at the temperature of maximum mass loss does not provide materials with a better mechanical performance compared to faster heating mode 3 with the linear heating. However, excessively high heating rates can result in material destruction.

Through the analysis of thermoset transformations during curing,

carbonization, and graphitization processes, it was found, that heat treatment leads to matrix densification by removal of non-carbon atoms and formation of a carbon structure through transformations of poly-aromatic 3D-network of phthalonitrile thermosets. The resulting carbon structure tends to be graphite-like and becomes more ordered after higher treatment temperature. After treatment at 2200 °C, phosphorus is completely eliminated from the matrix without damaging the structure, resulting in the formation of fully carbon material.

Thus, a novel approach to using an easy-processable phthalonitrile resin in C/C composites provides a fabrication of a uniform high-performance material in 4 cycles of reimpregnation-carbonization. Additional graphitization improves the material, especially the thermal properties. As can be seen, the comparisons between the present results and the structures of carbon materials obtained from other phthalonitriles reveal fundamental insights into the transformation process within a carbon matrix. Thus, these findings can be extrapolated to the carbonization of any phthalonitrile resin, including bio-based phthalonitrile resins [17,49,75,79]. Although, implementation of the fabrication method necessitates low-viscosity resins suitable for vacuum infusion, a characteristic that is only featured to a very limited number of the reported resins.

CRediT authorship contribution statement

Vladislav Aleshkevich: Conceptualization, Data curation, Writing – original draft, Visualization, Investigation, Formal analysis, Methodology. **Oleg Morozov:** Data curation, Writing – review & editing, Validation, Formal analysis, Supervision. **Alexander Babkin:** Funding acquisition, Resources. **Alexey Kepman:** Funding acquisition, Resources. **Boris Bulgakov:** Conceptualization, Data curation, Writing – review & editing, Investigation, Validation, Formal analysis,

Table 9

The crystalline parameters of PN-1000 and PN-2200.

	d_{002} , Å	L_{c2} , Å	L_{a3} , Å	I_D/I_G
PN-1000	3.7	10.3	18.5	2.38
PN-2200	3.5	26.6	70	0.63
Phthalonitriles, carbonized at 1000 °C [17] and 800 °C [53]	3.56 [17]	–	15.6 [17]	2.783 [17] 2.50 [53]
Mesophase Pitch, carbonized at 1100 °C [63]	3.56–3.58	13.66–16.49	–	–

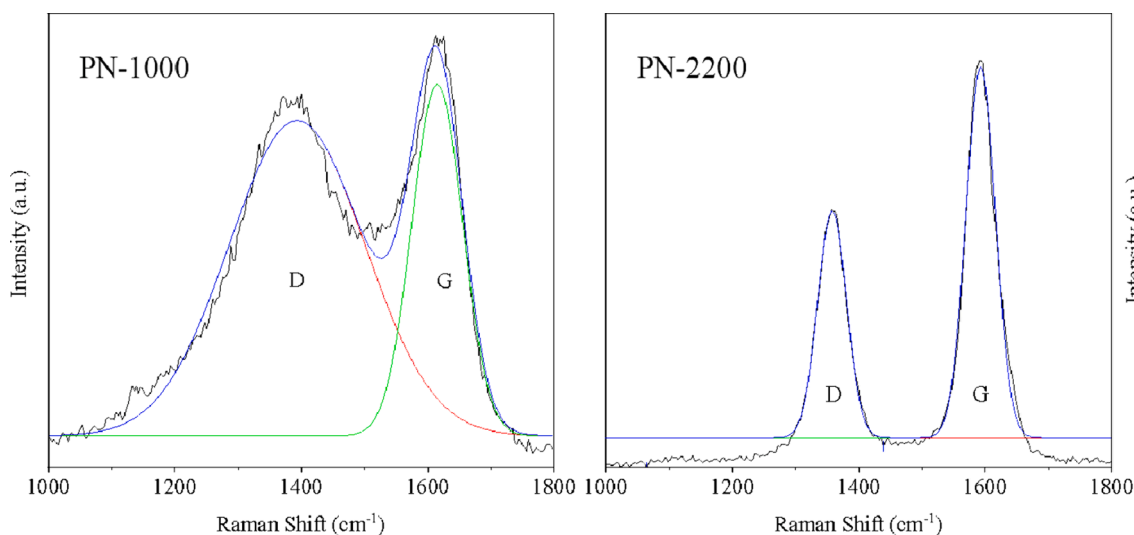


Fig. 14. Raman spectra of PN-1000 and PN-2200.

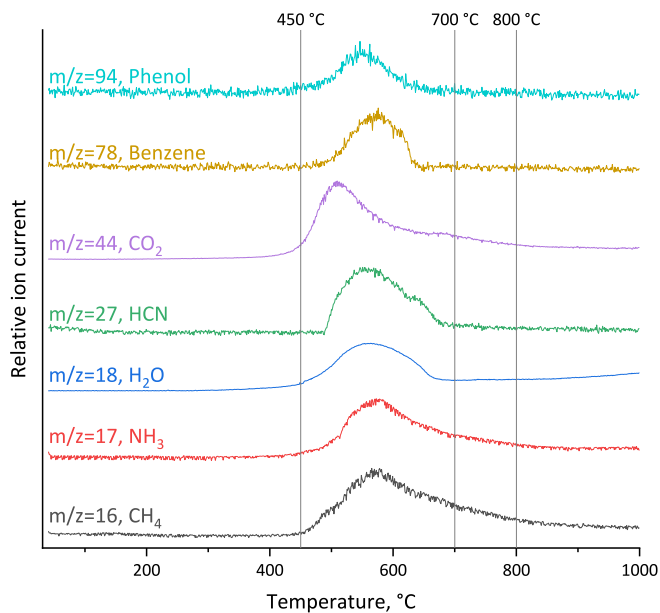


Fig. 15. Ion currents changes for gases evolving in TGA analysis of PN-375.

Supervision, Project administration.

Declaration of competing interest

The authors declare the following financial interests/personal relationships which may be considered as potential competing interests: Vladislav Aleshkevich reports financial support was provided by Russian Science Foundation. If there are other authors, they declare that they have no known competing financial interests or personal relationships that could have appeared to influence the work reported in this paper.

Data availability

Data will be made available on request.

Acknowledgements

This work was funded by the Russian Science Foundation, grant No. 22-13-00449.

Appendix A. Supplementary data

Supplementary data to this article can be found online at <https://doi.org/10.1016/j.compositesa.2024.108201>.

References

- Dwivedi H, Mathur RB, Dhani TL, Bahl OP, Monthieux M, Sharma SP. Evidence for the benefit of adding a carbon interphase in an all-carbon composite. *Carbon N Y* 2006;44:699–709.
- Manocha LM. Introduction of nanostructures in carbon-carbon composites. *Mater Sci Eng A* 2005;412:27–30.
- Tzeng SS, Chr YG. Evolution of microstructure and properties of phenolic resin-based carbon/carbon composites during pyrolysis. *Mater Chem Phys* 2002;73:162–9.
- Chung D. Carbon fiber composites. Elsevier; 2012.
- Pierson HO. Handbook of carbon, graphite, diamond, and fullerenes: properties, processing, and applications. Noyes Publications; 1993.
- Qi H, Liu Y, Wu L, Liu C, Ni S, Liu Q, et al. Mg-HA-C/C composites promote osteogenic differentiation and repair bone defects through inhibiting miR-16. *Front Bioeng Biotechnol* 2022;10:41.
- Fitzer E, Manocha LM. Carbon reinforcements and carbon/carbon composites. Berlin, Heidelberg: Springer, Berlin Heidelberg; 1998.
- Qingliang S, Hejun L, Lu L, Yunyu L, Qiangang F, Hongjiao L, et al. SiC nanowire reinforced carbon/carbon composites with improved interlaminar strength. *Mater Sci Eng A* 2016;651:583–9.
- Xue LZ, Li KZ, Jia Y, Zhang SY, Cheng J, Guo J. Flexural fatigue behavior of 2D cross-ply carbon/carbon composites at room temperature. *Mater Sci Eng A* 2015; 634:209–14.
- Manocha LM, Bhatt H, Manocha SM. Development of carbon/carbon composites by co-carbonization of phenolic resin and oxidised pan fibers. *Carbon N Y* 1996;34: 841–9.
- Anilias K, Surendranathan AO. Carbon-carbon composites – a review. *UPI J Eng Technol* 2018;1:8–19.
- Zaman W, Li KZ, Ikram S, Li W, Zhang DS, Guo LJ. Morphology, thermal response and anti-ablation performance of 3D-four directional pitch-based carbon/carbon composites. *Corros Sci* 2012;61:134–42.
- Derradji M, Jun W, Wenbin L, Wang J, Liu W. Phthalonitrile resins and composites: properties and applications. 1st ed. Elsevier; 2018.
- Bulgakov BA, Morozov OS, Timoshkin IA, Babkin AV, Kepman AV. Bisphthalonitrile-based thermosets as heat-resistant matrices for fiber reinforced plastics. *Polym Sci – Series C* 2021;63:64–101.
- Gu H, Gao C, Du A, Guo Y, Zhou H, Zhao T, et al. An overview of high-performance phthalonitrile resins: fabrication and electronic applications. *J Mater Chem C Mater* 2022;10:2925–37.
- Derradji M, Zegaoui A, Medjahed A, Liu W, Henniche A. Hybrid phthalonitrile-based materials with advanced mechanical and nuclear shielding performances. *Polym Compos* 2020;41:134–41.
- Xiao H, Zhou T, Lv J, He X, Chen M, Zeng K, et al. A high-mechanical-strength carbon/graphene porous composite with improved EMI shielding derived from high nitrogen-containing bio-based adenine-containing phthalonitrile resin. *J Electron Mater* 2022;51:5120–33.
- Augustine D, Chandran MS, Mathew D, Reghunadhan Nair CP. Polyphthalonitrile resins and their high-end applications. *Thermosets*: Elsevier; 2018. p. 577–619.
- Wu Z, Wang S, Zong L, Li N, Wang J, Jian X. Novel phthalonitrile-based composites with excellent processing, thermal, and mechanical properties. *High Perform Polym* 2018;30:720–30.
- Matthew Laskoski, Teddy M. Keller. Manufacturing of phthalonitriles derived from polyphenols as matrix materials for advanced composites for applications such as radomes, airframes, and electronics. US 2016/0311976 A1; 2016.
- Wu M, Xu J, Bai S, Chen X, Yu X, Naito K, et al. A high-performance functional phthalonitrile resin with a low melting point and a low dielectric constant. *Soft Matter* 2020;16:1888–96.
- Phua EJR, Liu M, Lim JSK, Cho B, Phthalonitrile-Based GCL, Packages E, et al. IEEE 20th electronics packaging technology conference (EPTC). IEEE 2018;2018: 537–42.
- Mehelli O, Derradji M, Belgacemi R, Zegaoui A, Khimeche K, Fantuzzi N, et al. Development of highly performant hybrid materials based on phthalonitrile resin for a simultaneous ballistic and nuclear shielding protection. *High Perform Polym* 2020;33:217–27.
- Derradji M, Mouloud A, Trache D, Zegaoui A, Medjahed A, Tarchoun AF, et al. Preparation and characterization of a new high-performance polymer composite and its application as a lead-free polymer-based projectile. *High Perform Polym* 2020;32:550–8.
- Dysart JL, Wolfgang JD, Smith AD, Atoyebi OF, Wallace JM, Maza WA, et al. Characterization of eumelanin as an additive in high-temperature phthalonitrile-based resin blends. *Macromol Chem Phys* 2023;224.
- Nechausov S, Aleksanova A, Morozov O, Babkin A, Kepman A, Avdeev V, et al. Heat-resistant phthalonitrile-based resins for 3D printing via vat photopolymerization. *ACS Appl Polym Mater* 2022;4:6958–68.
- Aleshkevich VV, Bulgakov BA, Lipatov YV, Babkin AV, Kepman AV. High performance carbon-carbon composites obtained by a two-step process from phthalonitrile matrix composites. *Mendelevov Commun* 2022;32:327–30.
- Fan Z, Ran Q, Xu X, Tang Y, Liu X, Jia K. A cross-linkable phthalonitrile derivative as a precursor to synthesize nitrogen-doped carbon nanodots for Ni ion detection. *New J Chem* 2023;47:22269–75.
- Yang X, Li Y, Lei W, Bai Z, Zhan Y, Li Y, et al. Understanding the thermal degradation mechanism of high-temperature-resistant phthalonitrile foam at macroscopic and molecular levels. *Polymers (Basel)* 2023;15:3947.
- Keller TM, Laskoski M, Saab A. Synthesis and Curing Additives for Phthalonitriles. US 8735532; 2014.
- Keller TM, Laskoski M, Saab AP. Controlling crosslinking density and processing parameters of phthalonitriles. US 2016/0168327; 2016.
- Wu Z, Li N, Han J, Wang C, Yuan K, Zeng Q, et al. Low-viscosity and soluble phthalonitrile resin with improved thermostability for organic wave-transparent composites. *J Appl Polym Sci* 2018;135:45976.
- Wang G, Guo Y, Han Y, Li Z, Ding J, Jiang H, et al. Enhanced properties of phthalonitrile resins reinforced by novel phthalonitrile-terminated polyaryl ether nitrile containing fluorene group. *High Perform Polym* 2020;32:3–11.
- Xu M, Chen S, Li X, Zhu S, Ren D, Liu X. Fabrication of phthalonitrile-based copper-clad laminates and their application properties: thermo-stability and dielectric properties. *Adv Ind Eng Polym Res* 2020;3:194–201.
- Sun BG, Shi HQ, Yang KX, Lei Q, Li YQ, Fu YQ, et al. Effects of 3-aminophenylacetylene on mechanical properties at elevated temperatures of carbon fiber/phthalonitrile composites. *Compos Commun* 2020;18:55–61.
- Gray GEF, Emerald J. Adair, Michael M. Liggett, Zhang D, Harris FW, A. R. Phthalonitrile Composites; 2006.
- Yakovlev MV, Kuchevskaia ME, Terekhov VE, Morozov OS, Babkin AV, Kepman AV, et al. Easy processable tris-phthalonitrile based resins and carbon

- fabric reinforced composites fabricated by vacuum infusion. *Mater Today Commun* 2022;33:104738.
- [38] Sun B-G-G, Lei Q, Guo Y, Shi H-Q-Q, Sun J-B-B, Yang K-X-X, et al. Enhanced mechanical properties at 400 °C of carbon fabric reinforced phthalonitrile composites by high temperature postcure. *Compos B Eng* 2019;166:681–7.
- [39] Lobanova MS, Aleshkevich VV, Yablokova MY, Morozov OS, Babkin AV, Kepman AV, et al. Kinetics of the oxidative aging of phthalonitrile resins and their effects on the mechanical properties of thermosets. *Thermochim Acta* 2023;724.
- [40] Lobanova M, Aleshkevich V, Babkin A, Kepman A, Avdeev V, Morozov O, et al. Effect of post-curing temperature on the retention of mechanical strength of phthalonitrile thermosets and composites after a long-term thermal oxidative aging. *Polym Compos* 2023.
- [41] Terekhov VE, Bogolyubov AA, Morozov OS, Afanaseva ES, Bulgakov BA, Babkin AV, et al. High-temperature phthalonitrile matrix containing silane fragments. *Mendelev Commun* 2020;30:796–8.
- [42] Tay YS, Liu M, Lim JSK, Chen H, Hu X. Phthalonitrile prepolymer and PAN blends: new strategy for precursor stabilization and pyrolytic char yield enhancement. *Polym Degrad Stab* 2020;172:109056.
- [43] Aleshkevich VV, Babkin AV, Avdeev VV. C/C composites developed from phthalonitrile based composites. *IOP Conf Ser Mater Sci Eng* 2019;683:12023.
- [44] Laskoski M, Keller TM, Qadri SB. Direct conversion of highly aromatic phthalonitrile thermosetting resins into carbon nanotube containing solids. *Polymer (Guildf)* 2007;48:7484–9.
- [45] Sastri SB, Armistead JP, Keller TM. Carbon-based composites derived from phthalonitrile resins. WO2000000350A1; 1998.
- [46] Dominguez DD, Jones HN, Keller TM. The effect of curing additive on the mechanical properties of phthalonitrile-carbon fiber composites. *Polym Compos* 2004;25:554–61.
- [47] Sastri SB, Armistead JP, Keller TM. Phthalonitrile-carbon fiber composites. *Polym Compos* 1996;17:816–22.
- [48] Gissinger JR, Zavada SR, Smith JG, Kemppainen J, Gallegos I, Odegard GM, et al. Predicting char yield of high-temperature resins. *Carbon N Y* 2023;202:336–47.
- [49] Guo X, Liang B, Chen M, He X, Xiao H, Zeng K, et al. Study on pyrolysis behavior of bio-based adenine containing phthalonitrile resin obtained by powder metallurgy-like process. *Polym Degrad Stab* 2021;188:109569.
- [50] Liang B, Wang J, Hu J, Li C, Li R, Liu Y, et al. TG-MS-FTIR study on pyrolysis behavior of phthalonitrile resin. *Polym Degrad Stab* 2019;169.
- [51] Liang B, Hu J, Yuan P, Li C, Li R, Liu Y, et al. Kinetics of the pyrolysis process of phthalonitrile resin. *Thermochim Acta* 2019;672:133–41.
- [52] Alenezi GT, Rajendran N, Abdel Nazeer A, Makhseed S. Development of uniform porous carbons from polycarbazole phthalonitriles as durable CO₂ adsorbent and supercapacitor electrodes. *Front Chem* 2022;10:879815.
- [53] Zeng J, Xie W, Zhou H, Zhao T, Bin XB, Jiang Q, et al. Nitrogen-doped graphite-like carbon derived from phthalonitrile resin with controllable negative magnetoresistance and negative permittivity. *Adv Compos Hybrid Mater* 2023;6: 1–12.
- [54] Babkin AV, Zodbinov EB, Bulgakov BA, Kepman AV, Avdeev VV. Low-melting siloxane-bridged phthalonitriles for heat-resistant matrices. *Eur Polym J* 2015;66: 452–7.
- [55] Babkin AV, Sulimov AV, Bulgakov BA, Kepman AV. Phosphorus-containing phthalonitrile resin for VIMP and RTM processing. In: SAMPE Conference Proceedings. Seattle, WA: Society for the Advancement of Material and Process Engineering; 2017. p. 713–24.
- [56] Bulgakov B, Sulimov A, Babkin A, Timoshkin I, Solopchenko A, Kepman A, et al. Phthalonitrile-carbon fiber composites produced by vacuum infusion process, vol. 51. London, England: SAGE Publications, UK; 2017.
- [57] Bulgakov BA, Babkin AV, Dzhevakov PB, Bogolyubov AA, Sulimov AV, Kepman AV, et al. Low-melting phthalonitrile thermosetting monomers with siloxane- and phosphate bridges. *Eur Polym J* 2016;84:205–17.
- [58] Terekhov VE, Aleshkevich VV, Afanaseva ES, Nechausov SS, Babkin AV, Bulgakov BA, et al. Bis(4-cyanophenyl) phenyl phosphate as viscosity reducing comonomer for phthalonitrile resins. *React Funct Polym* 2019;139:34–41.
- [59] Monzel WJ, Lu GQ, Prun TL, Houser CL, Yee GT. Thermal and oxidative behavior of a tetraphenylsilane-containing phthalonitrile polymer. *High Perform Polym* 2019;31:935–47.
- [60] Heinrich C, Aldridge M, Wineman AS, Kieffer J, Waas AM. Integrated computational materials science and engineering of textile polymer composites. Collection of technical papers - AIAA/ASME/ASCE/AHS/ASC structures, structural dynamics and materials conference; 2011. p. 33.
- [61] Devi GR, Rao KR, Rao KR. Carbon Carbon composites: an overview. *Def Sci J* 1993; 43:369–83.
- [62] Jia J, Ju J, Liu S, Ji G. Preparation and mechanical properties of C/C composites reinforced with arrayed SiC columnar pins. *Ceram Int* 2021;47:24262–9.
- [63] Yang J-Y, Park J-H, Kuk Y-S, Kim B-S, Seo M-K. One-step densification of carbon/carbon composites impregnated with pyrolysis fuel oil-derived mesophase binder pitches. C — *J Carbon Res* 2020;6:5.
- [64] Matzinos PD, Patrick JW, Walker A. Coal-tar pitch as a matrix precursor for 2-D C/C composites. *Carbon N Y* 1996;34:639–44.
- [65] Titirici MM, White RJ, Brun N, Budarin VL, Su DS, Del Monte F, et al. Sustainable carbon materials. *Chem Soc Rev* 2015;44:250–90.
- [66] Ji S, Yuan P, Hu J, Sun R, Zeng K, Yang G. A novel curing agent for phthalonitrile monomers: curing behaviors and properties of the polymer network. *Polymer (Guildf)* 2016;84:365–70.
- [67] Laskoski M, Neal A, Keller TM, Dominguez D, Klug CA, Saab AP. Improved synthesis of oligomeric phthalonitriles and studies designed for low temperature cure. *J Polym Sci A Polym Chem* 2014;52:1662–8.
- [68] Liu Y, Liu Z Zhou, Peng W Feng, Lu Z, Hu J Huai, Zeng K, et al. Inspiration from a new lignin-derived phthalonitrile resin: Unique curing behavior, and thermal properties. *Eur Polym J* 2019;121.
- [69] Kühl O. Phosphorus-31 NMR spectroscopy: a concise introduction for the synthetic organic and organometallic chemist. Springer; 2008.
- [70] Puziy AM, Poddubnaya OI, Gawdzik B, Sobiesiak M, Sprynskyy M. Structural evolution of polyimide-derived carbon during phosphoric acid activation. *C (Basel)* 2022;8:47.
- [71] Greenwood NN, Earnshaw A. Chemistry of the elements. 2nd ed. Oxford: Butterworth; 1998.
- [72] Freitas JCC, Bonagamba TJ, Emmerich FG. Investigation of biomass-and polymer-based carbon materials 13 using C high-resolution solid-state NMR. vol. 39; 2001.
- [73] Puziy AM, Poddubnaya OI, Socha RP, Gurgul J, Wisniewski M. XPS and NMR studies of phosphoric acid activated carbons. *Carbon N Y* 2008;46:2113–23.
- [74] Wang S, Jing X, Wang Y, Si J. High char yield of aryl boron-containing phenolic resins: the effect of phenylboronic acid on the thermal stability and carbonization of phenolic resins. *Polym Degrad Stab* 2014;99:1–11.
- [75] Zhou T, Xiao H, Peng W, Liang B, Liu Y, Lv J, et al. Study on pyrolysis behaviors of L-tyrosine-based phthalonitrile resin. *Polym Test* 2020;86:106506.
- [76] Huang Y, Liu H, Yuan H, Zhuang X, Yuan S, Yin X, et al. Association of chemical structure and thermal degradation of lignins from crop straw and softwood. *J Anal Appl Pyrolysis* 2018;134:25–34.
- [77] Sastri SB, Armistead JP, Keller TM. Carbonization of high-temperature resins. vol. 31; 1993.
- [78] Yang J, Chen H, Zhao W, Zhou J. TG-FTIR-MS study of pyrolysis products evolving from peat. *J Anal Appl Pyrolysis* 2016;117:296–309.
- [79] Xiao H, Zhou T, Shi M, Lv J, Li R, Zeng K, et al. A molding-sintering method inspired by powder metallurgy for thermosetting resins with narrow processing window: a case study on bio-based adenine containing phthalonitrile. *Chem Eng J* 2020;398:125442.